



## RESEARCH ARTICLE

# Imaging genomics discovery of a new risk variant for Alzheimer's disease in the postsynaptic SHARPIN gene

Sourena Soheili-Nezhad<sup>1,2,3</sup>  | Neda Jahanshad<sup>4</sup> | Sebastian Guelfi<sup>5</sup> |  
 Reza Khosrowabadi<sup>6</sup> | Andrew J. Saykin<sup>7,8,9</sup>  | Paul M. Thompson<sup>4</sup> |  
 Christian F. Beckmann<sup>2,3,10</sup> | Emma Sprooten<sup>2</sup> | Mojtaba Zarei<sup>1</sup> | the Alzheimer's  
 Disease Neuroimaging

<sup>1</sup>Institute of Medical Science and Technology, Shahid Beheshti University, Tehran, Iran

<sup>2</sup>Donders Institute for Brain, Cognition and Behaviour, Department of Cognitive Neuroscience, Radboud University Medical Centre, Nijmegen, The Netherlands

<sup>3</sup>Donders Centre for Cognitive Neuroimaging, Radboud University, Nijmegen, The Netherlands

<sup>4</sup>Imaging Genetics Center, USC Stevens Neuroimaging and Informatics Institute, Keck School of Medicine of USC, University of Southern California, Marina del Rey, California

<sup>5</sup>Reta Lila Weston Research Laboratories, Department of Molecular Neuroscience, University College London (UCL) Institute of Neurology, London, UK

<sup>6</sup>Institute for Cognitive and Brain Science, Shahid Beheshti University, Tehran, Iran

<sup>7</sup>Center for Neuroimaging, Department of Radiology and Imaging Sciences, Indiana University School of Medicine, Indianapolis, Indiana

<sup>8</sup>Indiana Alzheimer Disease Center, Indiana University School of Medicine, Indianapolis, Indiana

<sup>9</sup>Department of Medical and Molecular Genetics, Indiana University School of Medicine, Indianapolis, Indiana

<sup>10</sup>Oxford Centre for Functional Magnetic Resonance Imaging of the Brain (FMRIB), Wellcome Centre for Integrative Neuroimaging, University of Oxford, Oxford, UK

## Correspondence

Mojtaba Zarei, Institute of Medical Science and technology, Shahid Beheshti University,

## Abstract

Molecular mechanisms underlying Alzheimer's disease (AD) are difficult to investigate, partly because diagnosis lags behind the insidious pathological processes. Therefore, identifying AD neuroimaging markers and their genetic modifiers may help study early mechanisms of neurodegeneration. We aimed to identify brain regions of the highest vulnerability to AD using a data-driven search in the AD Neuroimaging Initiative (ADNI,  $n = 1,100$  subjects), and further explored genetic variants affecting this critical brain trait using both ADNI and the younger UK Biobank cohort ( $n = 8,428$  subjects). Tensor-Based Morphometry (TBM) and Independent Component Analysis (ICA) identified the limbic system and its interconnecting white-matter as the most AD-vulnerable brain feature. Whole-genome analysis revealed a common variant in SHARPIN that was associated with this imaging feature ( $rs34173062$ ,  $p = 2.1 \times 10^{-10}$ ). This genetic association was validated in the UK Biobank, where it was correlated with entorhinal cortical thickness bilaterally ( $p = .002$  left and  $p = 8.6 \times 10^{-4}$  right), and with parental history of AD ( $p = 2.3 \times 10^{-6}$ ). Our findings suggest that neuroanatomical variation in the limbic system and AD risk are associated with a novel variant in SHARPIN. The role of this postsynaptic density gene product in  $\beta 1$ -integrin adhesion is in line with the amyloid precursor protein (APP) intracellular signaling pathway and the recent genome-wide evidence.

## KEYWORDS

Alzheimer's disease, brain atrophy, independent component analysis, synaptic adhesion, tensor-based morphometry, whole-genome sequencing

Daneshjou Boulevard, 19839-69411, Tehran, Iran.  
Email: moj\_zarei@sbu.ac.ir

#### Funding information

Biogen, Grant/Award Number: PO 969323; National Institutes of Health (NIH), Grant/Award Numbers: R01 AG059871, R56 AG058854; Radboud Universitair Medisch Centrum, Grant/Award Number: Hypatia R0003664

## 1 | INTRODUCTION

AD is one of the leading causes of death and disability in the elderly for which no disease-modifying treatment yet exists. Thus far, interventional trials to slow the progression of AD have failed (Cummings, 2018). The mild and heterogeneous presentation at the early stage of AD reduces the accuracy of the available diagnostic criteria, which prevents timely initiation of potentially effective therapies. Advancement in the development of noninvasive biomarkers is expected to aid in early diagnosis and prognostic stratification of AD.

A number of MRI measures have been suggested to have potential for AD diagnosis and longitudinal monitoring. These include loss of hippocampal volume (Schuff et al., 2009), reduced thickness of the entorhinal cortex (Velayudhan et al., 2013) and increased volume of the lateral ventricles (Nestor et al., 2008). Most of these imaging features were chosen based on a priori assumptions of the boundaries of anatomical structures involved in the disease process. However, the sensitivity of a priori-driven approaches that single out a particular brain region such as the hippocampus is limited by heterogeneity of AD, which translates to different patterns of brain degeneration in different patients (Marquand, Rezek, Buitelaar, & Beckmann, 2016). The region-of-interest studies also disregard the spatial continuity across brain areas (Haak, Marquand, & Beckmann, 2018) and the covariance within and across brain networks (Xu, Groth, Pearson, Schretlen, & Calhoun, 2009). Exploratory methods such as independent component-analysis (ICA) can circumvent this problem, by providing a data-driven picture of the affected brain networks, and thereby track the impact of the disease in a hypothesis-free manner. Instead of imposing categorical or binary boundaries onto the data, feature extraction methods like ICA transform the data into features based on the inherent—in this case spatial—structure of the data. Staying closer to the inherent biological data structure allows more relevant variance to be maintained, which benefits the sensitivity of subsequent analyses. ICA also reduces the number of statistical tests without resorting to a priori regions of interest, which in most scenarios would substantially boost statistical power in the face of multiple testing. This is particularly true for genome-wide association studies of millions of variants. At the same time ICA also aids interpretability of high-dimensional data, by describing the data in terms of a smaller number of relevant variables (i.e., components or features).

AD is highly heritable at  $h^2 = 0.58\text{--}0.79$  (Gatz et al., 2006). APOE4, which is the strongest genetic risk factor for sporadic late-onset AD, explains only a quarter of this genetic variance. The novel

risk variants discovered by genome-wide association studies (GWAS) explain an even smaller proportion of AD heritability (Jansen et al., 2019). These studies commonly rely on diagnostic instruments for the dichotomous definition of the disease versus the healthy state. However, diagnostic instruments are originally aimed at guiding decisions in the clinic and capture mostly the terminal events of the disease pathways. Pathological brain changes are often reflected in neuroimaging data prior to the onset of clinical signs (Piers, 2018; Tabatabaei-Jafari, Shaw, Walsh, Cherbuin, & Initiative, 2019). Quantitative neuroimaging may therefore be more sensitive to the genetic determinants of AD at early stages, when the clinical presentation does not yet fulfill the diagnostic criteria.

Here, we used ICA of pre-processed structural brain MRI data in a longitudinal cohort of elderly subjects to arrive at a data-driven pattern of brain degeneration in AD and mild cognitive impairment (MCI). We then performed a genome-wide search for genetic variants associated with structural integrity of this disease-related brain feature. Finally, we validated the genome-wide association with structure of the medial temporal cortex in an independent sample. The effect of the variant on parental history of AD, as a proxy to dementia predisposition, was also assessed.

## 2 | METHODS

### 2.1 | ADNI participants

Imaging, whole-genome sequencing and clinical data used in the discovery phase of this study were obtained from the ADNI database (adni.loni.usc.edu). ADNI is a multi-center initiative led by principal investigator Michael W. Weiner, MD, VA Medical Center and University of California, San Francisco, and enrolls subjects with normal cognition, MCI and AD. Our investigation included 1,100 ADNI individuals (age:  $74.0 \pm 7.1$  year, Table 1) with baseline T1-weighted brain MRI scans. Longitudinal MRI scans were available in a subsample of 1,039 subjects

**TABLE 1** Study subjects

	CN	MCI	AD	Total (female)
Cross-sectional	383	456	361	1,100 (491)
Longitudinal	269	422	348	1,039 (457)
GWAS	226	402	180	808 (363)

who underwent follow-up imaging at  $1.07 \pm 0.08$  year ( $n = 1,009$  subjects) and/or  $2.07 \pm 0.11$  year intervals ( $n = 883$  subjects).

Cognitively healthy individuals were defined by Mini Mental State Examination (MMSE) scores between 24 and 30, CDR of zero, and by the absence of depression, dementia, and any sign of cognitive impairment. MCI subjects were defined by MMSE scores between 24 and 30, memory complaints with objective memory loss as measured by education-adjusted scores on Wechsler Memory Scale-Revised (WMS-R) logical memory II, a CDR of 0.5, absence of significant impairment in other cognitive domains and absence of dementia. AD patients had MMSE score between 20 and 26, CDR of 0.5 or 1.0 and fulfilled NINCDS/ADRDA criteria for probable AD.

## 2.2 | UK Biobank

The UK Biobank dataset was used for validation of our ADNI analysis results (Sudlow et al., 2015) including subjects with the age at baseline range of 40–69 years. Association of brain imaging-derived phenotypes (IDPs) with genome-wide variants has been previously investigated in 8,428 subjects scanned by MRI and data is publically available across 11,734,353 SNPs (Elliott et al., 2018). For our work, we extracted summary statistics of cortical thickness (<http://big.stats.ox.ac.uk>) for the top-hit variant of the ADNI association study in UK Biobank and visualized it on a standard FreeSurfer parcellation atlas. In addition, genome-wide statistics of the paternal ( $n = 292,053$  subjects) and maternal ( $n = 308,780$  subjects) history of AD were retrieved from an independent GWAS of UK Biobank cohort ([https://github.com/nealelab/uk\\_biobank\\_gwas](https://github.com/nealelab/uk_biobank_gwas)). We performed a fixed-effect meta-analysis on the maternal and paternal SNP effect sizes and obtained genome-wide variants associated with history of AD in parents, similar to the recent AD-by-proxy approach (Jansen et al., 2019; Marioni et al., 2018).

## 2.3 | Brain atrophy estimation and diagnosis discrimination using independent component analysis

We registered all MRI volumes to construct a minimum-deformation study brain template in four linear and four nonlinear iterations using SyN (Avants et al., 2010). Cross-sectional TBM was used to identify voxel-wise brain volume differences at baseline across 1,100 study subjects. Longitudinal tensor-based morphometry (TBM) was also performed to calculate voxel-wise progression of brain atrophy and its annual rate in all individuals with follow-up MRI scans ( $n = 1,039$ ), using extensively validated methods (Figure 1) (Yushkevich et al., 2010). Both of the cross-sectional and longitudinal pipelines yielded SyN Jacobian determinant maps, which respectively reflect voxel-wise differences in regional brain volume of each subject compared to the common template at baseline, or the annual rate of brain volume loss in each subject in course of the disease. The average maps of the longitudinal rates of change for each diagnostic group are shown in Figure S1. These Jacobian maps were then decomposed into independent sources by ICA.

ICA is an exploratory method for linearly decomposing neuroimaging data into 3D spatial maps and subject-wise loadings, and has shown to effectively separate neural processes of different origins in functional (Beckmann & Smith, 2004) and structural neuroimaging (Groves, Beckmann, Smith, & Woolrich, 2011). To decompose maps of structural brain variation at various spatial details, ICA was performed at multiple dimensions (8, 12, 16, 20, 24, 28, 32, 40, 48, 56, 64, 72, 80, 88 and 96), yielding a total of 1,348 spatial maps of baseline brain volume ( $n = 684$  maps) and of longitudinal atrophy ( $n = 664$  maps). The extracted components represent brain regions with structural covariance across the study population, that is, areas that tend to lose volume with statistically correlated trajectories possibly due to a common underlying pathology. In ICA, subject-wise loading values linearly reflect each subject's level of brain volume (in cross-sectional morphometry) or atrophy rate (in longitudinal morphometry) within each 3D spatial map (for further details, see Appendix S1). To find out which of the brain components were related to AD, they were used as predictor variables in L1-regularized (LASSO) logistic regression models (Tibshirani, 1996) to discriminate AD patients or MCI subjects from the cognitively normal group (Figure S2). Leave-one-out cross validation was used to optimize the L1 regularization parameter ( $\lambda$ ) and achieve maximum classification accuracy in the dichotomous case/control logistic discriminations. Regression beta estimates (log odds ratios) were then compared across all brain components to identify the single component with the highest association with AD in cross-sectional and longitudinal data, controlling for subjects' age and sex.

### 2.3.1 | Correlation of MRI feature with clinical ADAS score

Correlation of the top AD-associated brain component was investigated with cognitive performance at baseline as measured by the ADAS-cog-13 scale (Skinner et al., 2012). The analysis was performed separately for baseline volume measure and longitudinal atrophy rate of the top component in AD ( $n = 361$  cross-sectional, 348 longitudinal) and MCI ( $n = 456$  cross-sectional, 422 longitudinal) subjects, controlling for age and sex covariates in a general linear model.

## 2.4 | Genome-wide association study

The AD-associated imaging feature was brought to genome-wide association analysis to identify genetic drives of structural brain deficits in disease-vulnerable regions. Whole-genome sequencing data was collected at an average depth of 30–40 $\times$  in 808 participants, from which a total of 38,566,438 single-nucleotide polymorphisms (SNPs) and 5,969,342 short insertion-deletions (indels) were called using Genome Analysis Toolkit (GATK) (DePristo et al., 2011; Saykin et al., 2015). Variants were filtered by considering minor phred quality score of 30, minor allele frequency of 0.01, minimum variant genotyping rate of 0.9 and

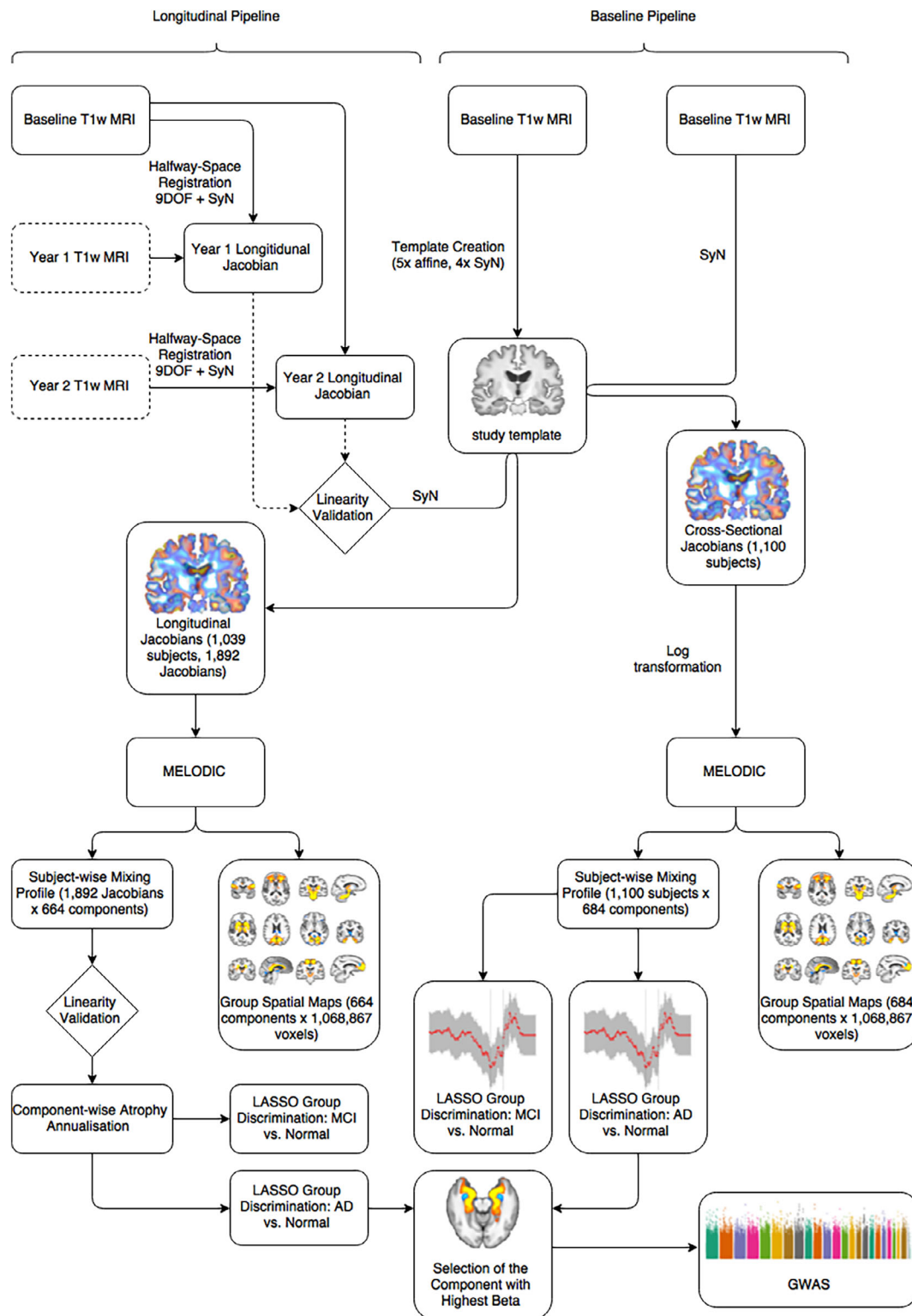


**FIGURE 1** Outline of the Study methods. T1-weighted MRIs were used to identify structural brain changes in cross-sectional and longitudinal studies. ICA decomposed 1,348 spatial sources of brain morphometry, among which the medial temporal circuit (MTC) was replicated as the top imaging predictor of AD and MCI and subsequently brought to GWAS

Hardy-Weinberg Equilibrium state of  $p > 1 \times 10^{-6}$ , resulting in inclusion of 10,957,927 QC-passed variants for whole-genome association. We chose the WGS data over the imputed DNA array genotypes for higher coverage and variant calling density of the former platform, as chip

arrays do not capture the total extent of genomic variation in each individual and some causal variants may be missed due to poor imputation. We searched for genetic variants correlated with baseline volume of the top AD-associated brain component in all study subjects (Table 1).

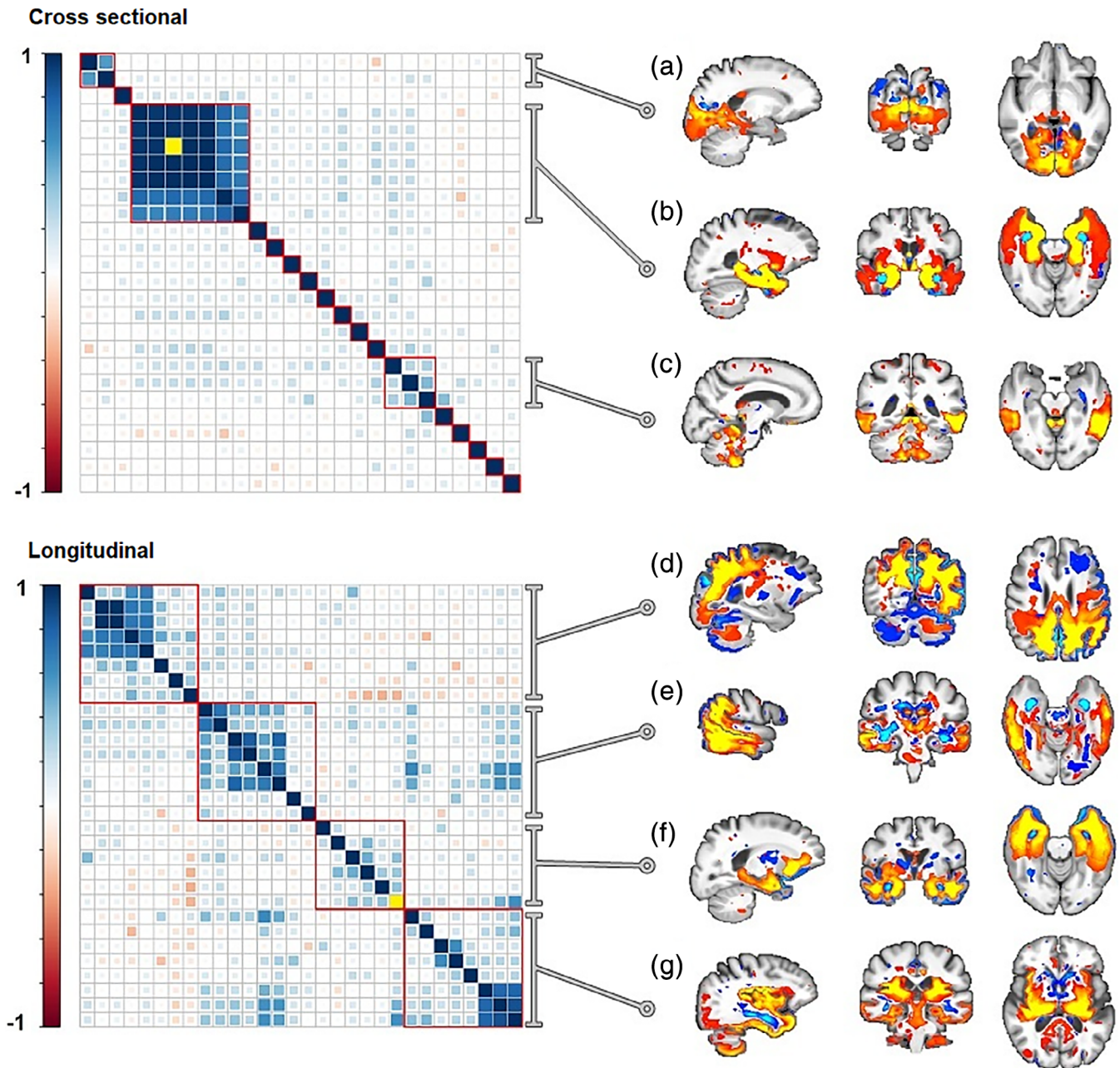


**FIGURE 2** Brain components related to Alzheimer's disease. Left: Cross-correlation matrices of brain components that discriminated AD patients from cognitively normal subjects were constructed. Hierarchical clustering was then applied to these matrices to group similar components together. Right: cluster-wise sum of the z-score maps of the components are shown (red-yellow: atrophy, blue: expansion; thresholded via mixture modeling). The strongest AD discriminator in both analyses was a component referred to as the medial temporal circuit (MTC) in this paper, which is plotted as the yellow diagonal element in both matrices. This component (see volume rendered video S1) was the focus of brain atrophy in a cluster of components mapping to temporal lobes (b and f). Brain morphometry results also showed other clusters of structural brain deficits in AD that map to the posterior brain/occipitoparietal regions (a, d) and lateral temporal, insular and subcortical areas (c, e, g)

The GWAS regression model included age, sex, the diagnosis groups (AD, MCI, cognitively normal), three principal axes of population structure, MRI pulse sequence (MP-RAGE vs. SPGR), and the APOE4 allele dosage as covariates. Our analysis showed that field strength, voxel-size, MRI vendor and the pulse sequence type (MP-RAGE vs. IR-SPGR) do not significantly affect the ICA phenotype, but we regress out the pulse sequence type from the data as it explained more variance than the rest.

### 3 | RESULTS

#### 3.1 | Strong structural covariance in Alzheimer's disease-affected brain regions: Independent component analysis

ICA identified latent sources in brain morphometry maps that mapped to anatomically and functionally coherent regions (Figure S3).

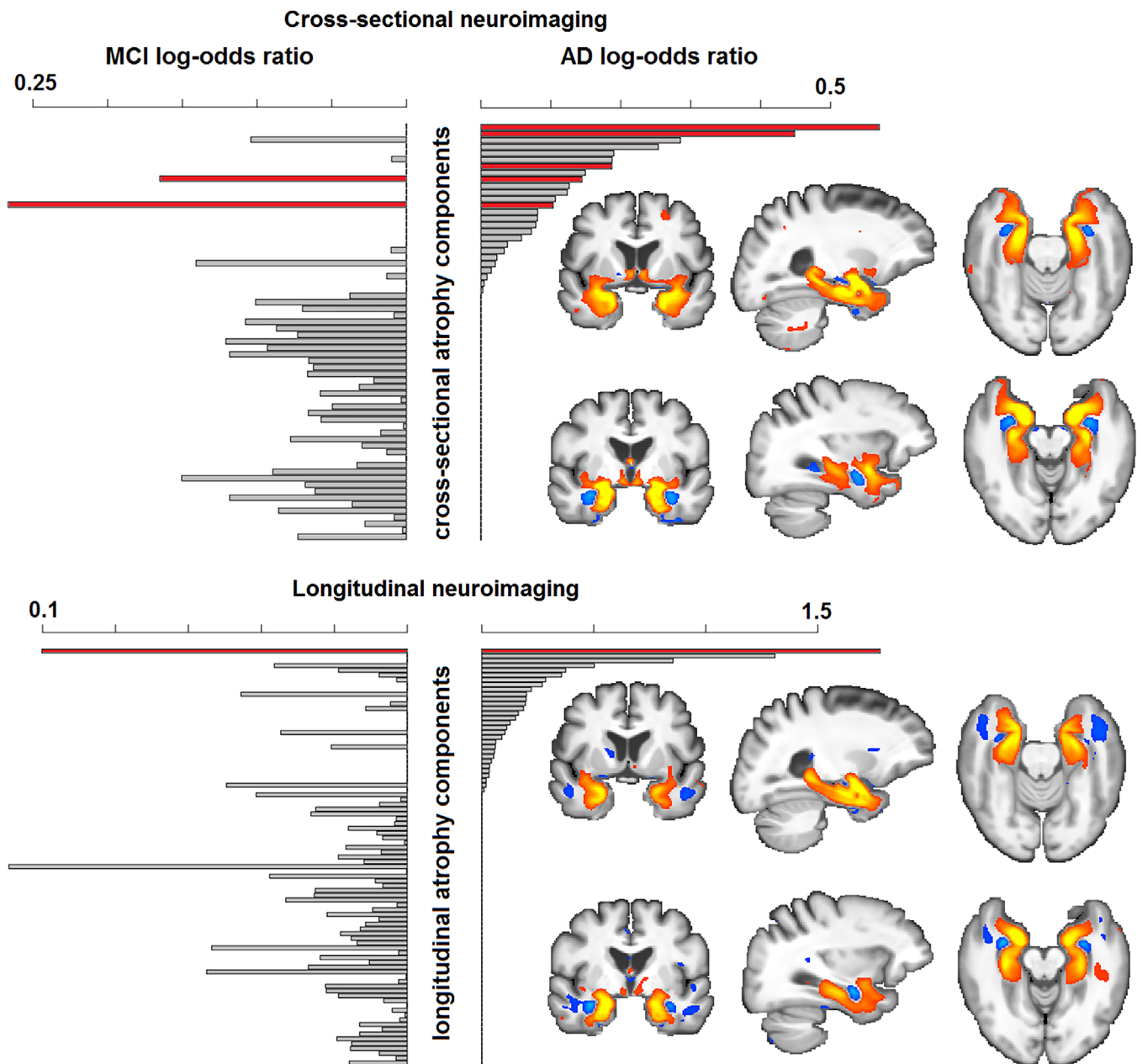


**FIGURE 3** Contribution of brain components in predicting subjects' cognitive status. Each bar represents a brain component that was able to distinguish MCI subjects (left plots) and/or AD patients (right plots) from the cognitively normal subjects in L1 regression models. Bar lengths encode log odds ratios reflecting the importance of each component in diagnosis classification. Both models in cross-sectional (top) and longitudinal neuroimaging (bottom) consistently identified the MTC component as the strongest predictor of AD and MCI (red bars). The top figure shows multiple bars reflecting the MTC, corresponding to different dimensionalities (See Appendix S1). Each voxel's contribution to the MTC is depicted in the figure on the right, for both the cross-sectional and the longitudinal decompositions

Following the two-class LASSO logistic regressions, AD patients could be classified by reduced volume of 26 brain components (out of 684) in cross-sectional MRI from the healthy group, or 30 components (out of 664) in longitudinal MRI, with respective classification accuracies of 86% and 87% as assessed by leave-one-out cross validation (Table 1). These component counts reflect the point of saturation in the LASSO regression model, that is, classification accuracy will no longer significantly increase by inclusion of more components (Figure S2). The cross-sectional components predicting AD diagnosis clustered to:

precuneus, occipital lobes and pulvinar (Figure 2a); a robust cluster including hippocampi, amygdalae, parahippocampal gyri, fornix, mammillary bodies, and uncinate fasciculi (Figure 2b); as well as lateral temporal lobes and the cerebellum (Figure 2c). The AD-predicting components in longitudinal TBM clustered to: precuneus, cuneus and occipito-parietal lobes (Figure 2d); thalamus, temporal lobes and its association areas (Figure 2e); medial temporal lobes, uncinate fasciculus and the orbitofrontal cortex (Figure 2f); as well as insula, basal ganglia and cerebellum (Figure 2g).

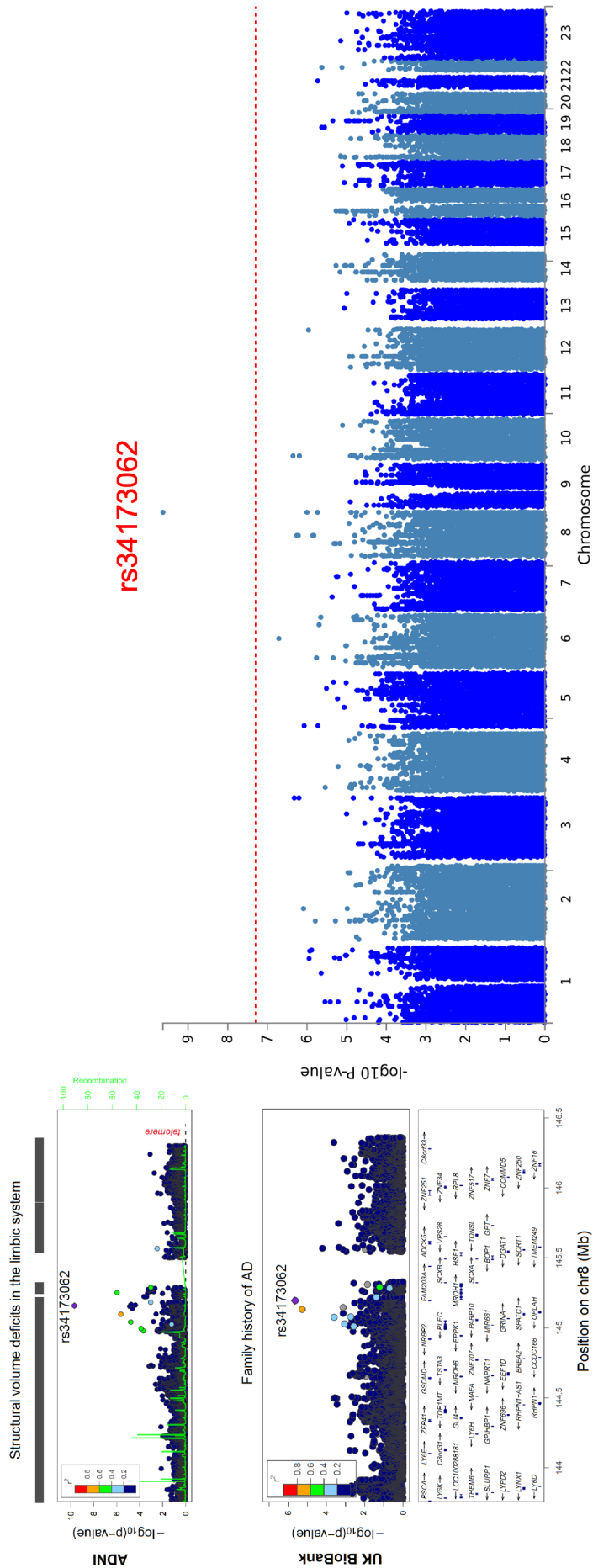


**FIGURE 4** Manhattan and regional association plots of the SHARPIN locus. Left: association of the SHARPIN locus with medial temporal lobe volume (ADNI) and parental history of AD (UK Biobank). Right: Manhattan plot showing genome-wide association of SHARPIN locus with medial temporal lobe volume in ADNI

### 3.2 | Early degeneration of the limbic system in Alzheimer's disease

The most prominent predictor of AD was a component that obtained the top odds-ratio rank in both the cross-sectional and the longitudinal analyses in discriminating AD from the cognitively-normal subjects. This component, referred to as the *Medial Temporal Circuit* (MTC) in this paper, was also a predictor of subjects with MCI, obtaining the top odds-ratio rank in discriminating MCI subjects from the cognitively normal group in cross-sectional brain morphometry (Figure 3). The MTC demonstrated a bilateral network-like topology (see video S1). The focus of brain atrophy in the MTC localized to the bilateral amygdalae, and further extended to the hippocampi, entorhinal cortex, insula, mammillary bodies, and the fornix.

Although the MTC included the hippocampus, it had a better discriminatory power for MCI subjects than hippocampus per se (Welch's  $t = 4.4$ :  $p = 1.2 \times 10^{-5}$  vs.  $t = 3.2$ :  $p = .002$  for MTC and hippocampus, respectively). The MTC also showed much higher

statistical power than hippocampal volume for group-wide discrimination of the AD from the cognitively normal group, although subject to circularity (Welch's  $t = 16.8$ :  $p < 10^{-15}$  vs.  $t = 4.4$ :  $p = 1.1 \times 10^{-5}$  for MTC and hippocampus, respectively).

### 3.3 | Reduction of brain volume in the medial temporal component and cognitive decline

Cognitive performance of participants, as measured by ADAS-cog, was correlated with MTC at its baseline volume in AD ( $p = 5.4 \times 10^{-8}$ ) and MCI ( $p = 9.6 \times 10^{-7}$ ), adjusted for age and sex. Similarly, the atrophy rate in MTC showed significant associations with ADAS-cog in AD ( $p = .04$ ) and MCI subjects ( $p = .002$ ) adjusted for age and sex. Older age ( $p = 2.6 \times 10^{-5}$ ) and female sex ( $p = 7.5 \times 10^{-5}$ ) were associated with faster atrophy in this imaging feature. Compared to the cognitively normal group, the annual atrophy rate in the MTC was increased by 2.1-fold in MCI and 5.1-fold in AD patients.

**TABLE 2** GWAS top SNPs

SNP	Chr	Position (hg19)	A1	A2 (effect)	Frequency	$\beta$	Gene mapping	$p$ -value
rs56112946 <sup>a</sup>	3	197,077,194	C	T	0.03	-.15	-	$3.1 \times 10^{-7}$
rs3778470	6	94,075,684	G	A	0.12	-.15	EPHA7 (intronic)	$1.5 \times 10^{-7}$
rs149101079	8	69,347,181	G	A	0.04	-.15	C8orf34	$3.1 \times 10^{-7}$
rs34173062	8	145,158,607	G	A	0.10	-.19	SHARPIN (missense)	$2.1 \times 10^{-10}$
rs28439901	10	14,494,941	G	A	0.08	-.15	FRMD4A (intronic)	$3.2 \times 10^{-7}$

<sup>a</sup>In linkage disequilibrium with rs55672024 ( $r^2 = .96$ ).

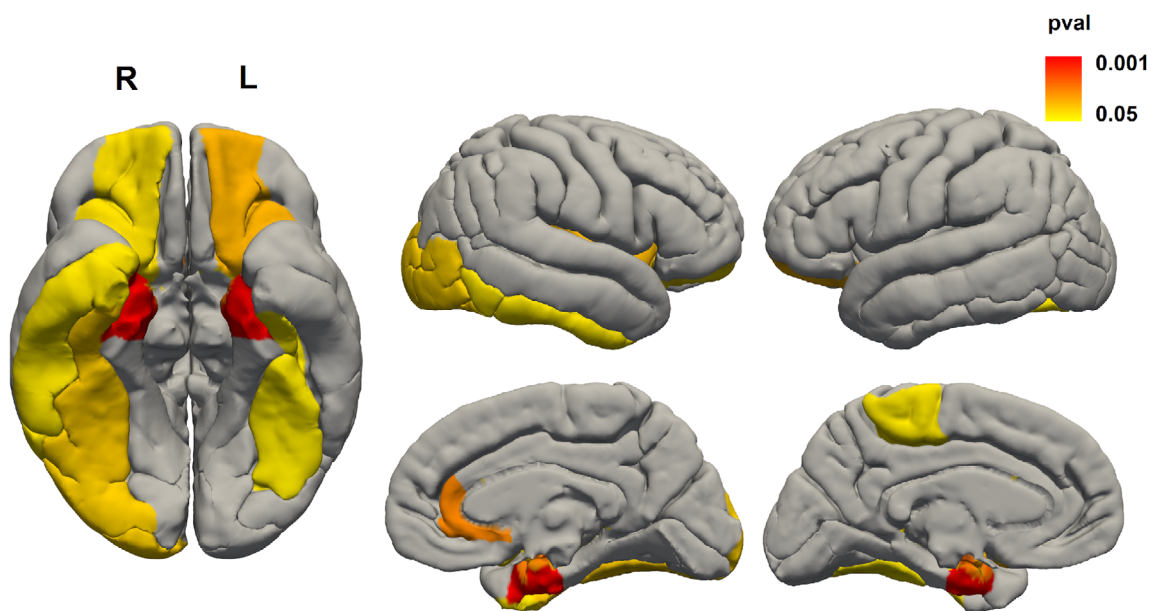


**FIGURE 5** Association of rs34173062 with cortical thickness. Thickness of bilateral entorhinal cortices (red) was significantly associated with rs34173062 in the UK Biobank cohort ( $n=8,428$  subjects)



### 3.4 | Genetic modifiers of brain volume in the medial temporal component

GWAS revealed a single missense SNP in the SHARPIN gene, rs34173062, which was genome-wide significant at  $p = 2.1 \times 10^{-10}$  (normalized beta =  $-2$ ; Figures 4 and S4). Genomic inflation ( $\lambda$ ) was calculated at 1.028. Two other trend-level variants ( $p < 10^{-6}$ ) were located in the introns of EPHA7 and FRMD4A (Table 2). The APOE locus was associated with the MRI feature at  $p = .0047$ . We tested 28 other AD risk loci of the latest AD GWAS (Jansen et al., 2019), and none of the risk variants passed multiple comparisons corrections. There were two weak signals for HLA-DRB1 and PICCALM loci at the same direction ( $p = .013$  and  $.026$  respectively), but general sign-concordance was a trend at  $p = .068$ . Performing the GWAS without conditioning on APOE $\epsilon$ 4 did not substantially affect the top variants statistics, and SHARPIN remained the single genome-wide significant locus at  $p = 6.3 \times 10^{-10}$ . MRI pulse sequence (MP-RAGE vs. IR-SPGR) did not affect the ICA-extracted measure ( $p = .8$ ). We sought validation of the SHARPIN variant in the UK Biobank cohort in which rs34173062 was directly genotyped by the Axiom genotyping array (Elliott et al., 2018), showing a minor allele frequency of 0.07. In this cohort ( $n = 8,428$  subjects), rs34173062 was associated with reduced thickness of the entorhinal cortex in left ( $p = .002$ ) and right ( $p = 8.6 \times 10^{-4}$ ) hemispheres, in the same direction as in the ADNI discovery sample (effect allele: A-allele; effect size on unit-variance normalized phenotype =  $-0.1$ , Figure 5). As the age of the UK Biobank subjects (49–69 years) is relatively young for clinical presentation of late-onset AD, we further searched for parental history of AD as a proxy to its heritable component. The risk allele (rs34173062-A) was significantly associated with increased maternal ( $p = .0012$ ) and paternal ( $p = 5.1 \times 10^{-4}$ ) history of AD, which translates to a fixed-effect meta-analysis p-value of  $2.3 \times 10^{-6}$  in both parents with a consistent effect direction (Figure 4, regional association plot).

## 4 | DISCUSSION

Using fully data-driven methods, we identified an anatomical feature of brain atrophy in AD, centered on the medial temporal lobes and its input/output circuits to fornix and the parahippocampal gyrus. Considering the role of this network and the associated pathways in memory mechanisms, observation of voxel-wise covariance in its subcomponents may reflect network-level vulnerability to a common underlying pathology in AD. This finding may be due to cellular and proteomic compositions driving brain degeneration and resulting in a symmetrical pattern of brain atrophy in the ICA probability maps. Specifically, our limbic component suggests that amygdalae are the most vulnerable structures of this network in AD, followed by bilateral hippocampi in a head-to-tail direction, and subsequently fimbriae and fornical tracts. This observation is consistent with a previous report showing that a healthy APOE4 carrier status is associated with abnormal brain connectivity in amygdalae and hippocampal heads,

suggesting early involvement of these subregions of the medial temporal lobes in the disease trajectory (Filippini et al., 2009).

Our results indicate that the parental AD-by-proxy phenotype is associated with a genetic modifier of a structurally disrupted limbic system as revealed by ICA and MRI. Similar to AD, the limbic component was the strongest imaging predictor of MCI, but the lower discriminatory power in MCI discrimination indicates that individuals with MCI are more similar to the healthy population in terms of this brain phenotype, and that they may represent a more heterogeneous population than the clinically probable AD group. Nevertheless, these observations support the notion that the underlying mechanisms of mild cognitive impairment partially overlap with AD. Clinical studies such as drug trials may benefit from stratifying MCI cohorts based on data-driven imaging features of limbic integrity at baseline.

In our genetic association analysis, we identified a common variant in SHARPIN in association with the MRI feature of the limbic system. This variant substitutes an amino acid in the N-terminal domain of the SHARPIN protein, a site responsible for its dimerization with potential roles in scaffolding as it adopts a pleckstrin homology superfold (Stieglitz, Haire, Dikic, & Rittinger, 2012). Association of this variant with the history of AD in both parents, in the UK Biobank as an independent cohort comprising younger population, confirms contribution of SHARPIN to dementia heritability and early subclinical pathology. Two recent articles have implicated SHARPIN in AD, with an ultra-rare variant in this gene at minor allele frequency of  $\sim 0.0002$  discovered to increase the risk of AD to almost six-fold in a Japanese cohort (Asanomi et al., 2019; Lancour et al., 2018). While this variant is not polymorphic in the western population, our study shows that another nonsynonymous variant in SHARPIN predisposes to AD and brain degeneration in the western population. The variant we observed is ultra-rare to nonpolymorphic in the eastern Asian cohorts ( $<0.01$ ), but has a minor allele frequency of 0.04–0.13 in northern American, European and Iranian populations (Fattahi et al., 2019). As a component of the postsynaptic SHANK scaffold, SHARPIN links the glutamate neurotransmitter receptors with the internal actin cytoskeleton (Lim et al., 2001). SHARPIN also modulates recruitment of another AD risk gene product, Kindlin-2, to the  $\beta$ 1-integrin adhesion receptors (Rantala et al., 2011). We suspect that SHARPIN affects synaptic adhesion and its dysfunction may disrupt the postsynaptic scaffold. Implication of the cell adhesion pathway by SHARPIN spotlights alternate mechanisms of APP and  $\gamma$ -secretase function in cell adhesion regulation, and specially direct interaction of APP with the  $\beta$ 1-integrin adhesion pathway (Bot, Schweizer, Ben Halima, & Fraering, 2011; Sabo, Ikin, Buxbaum, & Greengard, 2001).

FRMD4A and EPHA7 loci were also associated with limbic degeneration in the discovery cohort at a trend-level ( $p < 10^{-6}$ ). FRMD4A has been previously associated with AD (Lambert et al., 2013) and codes for a scaffolding protein that connects the actin cytoskeleton with adherens junctions for cell adhesion regulation and membrane remodeling (Ikenouchi & Umeda, 2010). Although the potential role of FRMD4A in neurobiology is unknown, this molecular function aligns with the mechanisms of postsynaptic adhesion and neurotransmitter

receptor trafficking in synaptic plasticity. EPHA7 codes for a receptor engaged in dendritic guidance and adhesion-regulated assembly of the synapse (Clifford et al., 2014), further highlighting the cytoskeletal pathway acting downstream to the synaptic adhesion receptors in AD. A rare variant in this gene has been previously reported to segregate with the disease status in a family with autosomal dominant AD (Kunkle B.W., 2014). Of note, both of these gene products interact with the  $\beta$ 1-integrin adhesion pathway, either through ARF and cytohesin (Oh & Santy, 2010) or directly (Sharfe et al., 2008).

While argument has been recently made for relevance of the focal adhesion pathway to elements of the amyloid cascade (Dourlen, Kilinc, Malmanche, Chapuis, & Lambert, 2019), we suspect that cell adhesion may rather act independently of the amyloid cascade in the disease process. In the context of cell adhesion, SHARPIN and APP share intriguing molecular signaling mechanisms with the APOE receptors. Both APP and SHARPIN cross-talk with the  $\beta$ 1-integrin pathway of cell adhesion (Rantala et al., 2011; Sabo et al., 2001) as does the APOE receptor LRP1 (Orr et al., 2003). A recent elegant report has revealed clock-like accumulation of somatic mutations in aging neurons of healthy humans, and this *genosenium* mechanism (Hoang et al., 2016; Lodato et al., 2018) may drive loss of critical synaptic adhesion regulators such as the extremely large LRP1B receptor of APOE, which has a highly brain specific expression profile paralleling areas of AD vulnerability (Haas et al., 2011; Marschang et al., 2004; Wu, Li, Yu, & Deng, 2008). Further investigation into the effect of genosenium on synaptic adhesion regulators and their modulation by the RELN/ $\beta$ 1-integrin/LRP pathway may be warranted in light of the genetic liability of AD that remains unexplained by amyloid beta-related mechanisms.

A major strength of our study is the use of ICA, which allowed us to derive a data-driven, voxel-wise neuroanatomical phenotype that is more sensitive to AD and MCI than the widely used hippocampal volume feature. For future researchers, it will be possible to map the AD-relevant brain component of the medial temporal lobes to other, independent cohorts, using the voxel-wise morphometry data and spatial regression to derive an AD-sensitive MRI feature. Another strength is the validation of our genome-wide significant association in a similar neuroanatomical region in an independent cohort. However, our study also has a number of limitations. It was not possible to use the clinical AD phenotype in the UK Biobank cohort due to the relatively young age distribution. The parental by-proxy phenotype used here is confounded by recall bias and relative lack of specificity. Nevertheless, a previous study has shown that this proxy phenotype has a high level of genetic correlation ( $r = .8$ ) with the genetic architecture of AD (Jansen et al., 2019). As a second limitation, further tracking the longitudinal trajectory of brain atrophy and its association with symptoms of cognitive decline will be needed to validate the ICA-based imaging feature of the limbic system as an early disease biomarker. We observed that except APOE, other risk loci of clinical AD were not associated with the structural MRI feature in our association study at a significant level. This divergence may either stem from limited statistical power, or indicate that brain atrophy and clinical

cognitive decline are biologically inter-related but not equivalent in their genetic underpinnings. MRI-derived atrophy features probably reflect neuronal death aspect of AD pathophysiology that results in loss of tissue. However, genetic risk factors of clinical AD may as well act through other pathways such as functionally impairing neurotransmission efficiency and synaptic disorganization that may not be strongly reflected in structural MRI. In a recent preprint the same SHARPIN variant has been reported as a risk locus of AD in a case/control study (de Rojas et al., 2020).

In conclusion, using a data-driven decomposition of brain morphometry maps, we identify early limbic degeneration as a new imaging feature of AD, and report a novel genetic risk variant in SHARPIN associated with structural deficits of this vulnerable brain region. Our multivariate method of mining brain degeneration using structural MRI and ICA may benefit future studies of AD, including disease prognosis and treatment trials. Our results underscore SHARPIN, as a postsynaptic adhesion modulator, in pathways of neurodegeneration in AD. Frequent implication of the  $\beta$ 1-integrin pathway by several novel risk genes of AD including SHARPIN warrants further research.

#### ACKNOWLEDGMENTS

Authors are thankful to Professor John Hardy and Professor Charles DeCarli for their useful comments. This work was supported in part by Radboudumc Hypatia Grant (R0003664 to E. S. and S. S.-N.), NIH grants R01 AG059871 (N. J.) and R56 AG058854 (P. M. T), and research related grant support from Biogen PO 969323 (N. J. and P. M. T). Data collection and sharing for this project was funded by the Alzheimer's Disease Neuroimaging Initiative (ADNI) (National Institutes of Health Grant U01 AG024904) and DOD ADNI (Department of Defense award number W81XWH-12-2-0012). ADNI is funded by the National Institute on Aging, the National Institute of Biomedical Imaging and Bioengineering, and through generous contributions from the following: AbbVie, Alzheimer's Association; Alzheimer's Drug Discovery Foundation; Araclon Biotech; BioClinica, Inc.; Biogen; Bristol-Myers Squibb Company; CereSpir, Inc.; Eisai Inc.; Elan Pharmaceuticals, Inc.; Eli Lilly and Company; EuroImmun; F. Hoffmann-La Roche Ltd. And its affiliated company Genentech, Inc.; Fujirebio; GE Healthcare; IXICO Ltd.; Janssen Alzheimer Immunotherapy Research & Development, LLC.; Johnson & Johnson Pharmaceutical Research & Development LLC.; Lumosity; Lundbeck; Merck & Co., Inc.; MesoScale Diagnostics, LLC.; NeuroRx Research; Neurotrack Technologies; Novartis Pharmaceuticals Corporation; Pfizer Inc.; Piramal Imaging; Servier; Takeda Pharmaceutical Company; and Transition Therapeutics. The Canadian Institutes of Health Research is providing funds to support ADNI clinical sites in Canada. Private sector contributions are facilitated by the Foundation for the National Institutes of Health ([www.fnih.org](http://www.fnih.org)). The grantee organization is the Northern California Institute for Research and Education, and the study is coordinated by the Alzheimer's Disease Cooperative Study at the University of California, San Diego. ADNI data are disseminated by the Laboratory for Neuro Imaging at the University of Southern California.

## CONFLICT OF INTERESTS

The authors declare that the research was conducted in the absence of any commercial or financial relationships that could be construed as a potential conflict of interest regarding the material presented in this manuscript.

## AUTHOR CONTRIBUTIONS

Sourena Soheili-Nezhad conceived and designed the study, wrote the manuscript, and analyzed the data. Emma Sprooten, and Mojtaba Zarei conceived and designed the study and wrote the manuscript. Neda Jahanshad, Sebastian Guelfi, Reza Khosrowabadi, Andrew J. Saykin, Paul M. Thompson, and Christian F. Beckmann provided revisions to scientific content of the manuscript.

## DATA AVAILABILITY STATEMENT

The data that support the findings of this study are available at the University of Southern California, Laboratory of Neuro Imaging ADNI repository (<http://adni.loni.usc.edu>). Public domain UK Biobank genome-wide association study summary statistics are available at the Oxford BIG server (<http://big.stats.ox.ac.uk>) and the Neale lab repositories (<http://www.nealelab.is/uk-biobank>).

## ORCID

Sourena Soheili-Nezhad  <https://orcid.org/0000-0002-3571-1270>

Andrew J. Saykin  <https://orcid.org/0000-0002-1376-8532>

## REFERENCES

- Asanomi, Y., Shigemizu, D., Miyashita, A., Mitsumori, R., Mori, T., Hara, N., ... Ozaki, K. (2019). A rare functional variant of SHARPIN attenuates the inflammatory response and associates with increased risk of late-onset Alzheimer's disease. *Molecular Medicine*, 25(1), 20. <https://doi.org/10.1186/s10020-019-0090-5>
- Avants, B. B., Yushkevich, P., Pluta, J., Minkoff, D., Korczykowski, M., Detre, J., & Gee, J. C. (2010). The optimal template effect in hippocampus studies of diseased populations. *NeuroImage*, 49(3), 2457–2466. <https://doi.org/10.1016/j.neuroimage.2009.09.062>
- Beckmann, C. F., & Smith, S. M. (2004). Probabilistic independent component analysis for functional magnetic resonance imaging. *IEEE Transactions on Medical Imaging*, 23(2), 137–152. <https://doi.org/10.1109/tmi.2003.822821>
- Bot, N., Schweizer, C., Ben Halima, S., & Fraering, P. C. (2011). Processing of the synaptic cell adhesion molecule neurexin-3beta by Alzheimer disease alpha- and gamma-secretases. *Journal of Biological Chemistry*, 286(4), 2762–2773. <https://doi.org/10.1074/jbc.M110.142521>
- Clifford, M. A., Athar, W., Leonard, C. E., Russo, A., Sampognaro, P. J., Van der Goes, M.-S., ... Donoghue, M. J. (2014). EphA7 signaling guides cortical dendritic development and spine maturation. *Proceedings of the National Academy of Sciences of the United States of America*, 111(13), 4994–4999. <https://doi.org/10.1073/pnas.1323793111>
- Cummings, J. (2018). Lessons learned from Alzheimer disease: Clinical trials with negative outcomes. *Clinical and Translational Science*, 11(2), 147–152.
- de Rojas, I., Moreno-Grau, S., Tesi, N., Grenier-Boley, B., Andrade, V., Jansen, I., ... Ruiz, A. (2020). Common variants in Alzheimer's disease: Novel association of six genetic variants with AD and risk stratification by polygenic risk scores. *medRxiv*, 19012021. <https://doi.org/10.1101/19012021>
- DePristo, M. A., Banks, E., Poplin, R., Garimella, K. V., Maguire, J. R., Hartl, C., ... Daly, M. J. (2011). A framework for variation discovery and genotyping using next-generation DNA sequencing data. *Nature Genetics*, 43(5), 491–498. <https://doi.org/10.1038/ng.806>
- Dourlen, P., Kilinc, D., Malmanc, N., Chapuis, J., & Lambert, J.-C. (2019). The new genetic landscape of Alzheimer's disease: From amyloid cascade to genetically driven synaptic failure hypothesis? *Acta Neuropathologica*, 138(2), 221–236. <https://doi.org/10.1007/s00401-019-02004-0>
- Elliott, L. T., Sharp, K., Alfaro-Almagro, F., Shi, S., Miller, K. L., Douaud, G., ... Smith, S. M. (2018). Genome-wide association studies of brain imaging phenotypes in UKbiobank. *Nature*, 562(7726), 210–216.
- Fattahi, Z., Beheshtian, M., Mohseni, M., Poustchi, H., Sellars, E., Nezhadi, S. H., ... Najmabadi, H. (2019). Iranome: A catalog of genomic variations in the Iranian population. *Human Mutation*, 40(11), 1968–1984. <https://doi.org/10.1002/humu.23880>
- Filippini, N., MacIntosh, B. J., Hough, M. G., Goodwin, G. M., Frisoni, G. B., Smith, S. M., ... Mackay, C. E. (2009). Distinct patterns of brain activity in young carriers of the APOE-epsilon4 allele. *Proceedings of the National Academy of Sciences of the United States of America*, 106(17), 7209–7214. <https://doi.org/10.1073/pnas.0811879106>
- Gatz, M., Reynolds, C. A., Fratiglioni, L., Johansson, B., Mortimer, J. A., Berg, S., ... Pedersen, N. L. (2006). Role of genes and environments for explaining Alzheimer disease. *Archives of General Psychiatry*, 63(2), 168–174. <https://doi.org/10.1001/archpsyc.63.2.168>
- Groves, A. R., Beckmann, C. F., Smith, S. M., & Woolrich, M. W. (2011). Linked independent component analysis for multimodal data fusion. *NeuroImage*, 54(3), 2198–2217. <https://doi.org/10.1016/j.neuroimage.2010.09.073>
- Haak, K. V., Marquand, A. F., & Beckmann, C. F. (2018). Connectopic mapping with resting-state fMRI. *NeuroImage*, 170, 83–94. <https://doi.org/10.1016/j.neuroimage.2017.06.075>
- Haas, J., Beer, A. G., Widschwendter, P., Oberdanner, J., Salzmann, K., Sarg, B., ... Marschang, P. (2011). LRP1b shows restricted expression in human tissues and binds to several extracellular ligands, including fibrinogen and apoE-carrying lipoproteins. *Atherosclerosis*, 216(2), 342–347. <https://doi.org/10.1016/j.atherosclerosis.2011.02.030>
- Hoang, M. L., Kinde, I., Tomasetti, C., McMahon, K. W., Rosenquist, T. A., Grollman, A. P., ... Papadopoulos, N. (2016). Genome-wide quantification of rare somatic mutations in normal human tissues using massively parallel sequencing. *Proceedings of the National Academy of Sciences*, 113(35), 9846–9851.
- Ikenouchi, J., & Umeda, M. (2010). FRMD4A regulates epithelial polarity by connecting Arf6 activation with the PAR complex. *Proceedings of the National Academy of Sciences of the United States of America*, 107(2), 748–753. <https://doi.org/10.1073/pnas.0908423107>
- Jansen, I. E., Savage, J. E., Watanabe, K., Bryois, J., Williams, D. M., Steinberg, S., ... Posthuma, D. (2019). Genome-wide meta-analysis identifies new loci and functional pathways influencing Alzheimer's disease risk. *Nature Genetics*, 51(3), 404–413. <https://doi.org/10.1038/s41588-018-0311-9>
- Kunkle, B. W., Hamilton, K. L., Perry, W. R., Carney, R. M., Whitehead, J. R., Gilbert, J. R., ... Haines, J. L. (2014). Whole-exome sequencing of multiplex families identifies several rare coding variants in known and novel Late-Onset Alzheimer genes. Presented at: The 64th Annual Meeting of The American Society of Human Genetics.
- Lambert, J.-C., Grenier-Boley, B., Harold, D., Zelenika, D., Chouraki, V., Kamatani, Y., ... Reitz, C. (2013). Genome-wide haplotype association study identifies the FRMD4A gene as a risk locus for Alzheimer's disease. *Molecular Psychiatry*, 18(4), 461–470.
- Lancour, D., Naj, A., Mayeux, R., Haines, J. L., Pericak-Vance, M. A., Schellenberg, G. D., ... Kasif, S. (2018). One for all and all for one: Improving replication of genetic studies through network diffusion. *PLoS Genetics*, 14(4), e1007306. <https://doi.org/10.1371/journal.pgen.1007306>

- Lim, S., Sala, C., Yoon, J., Park, S., Kuroda, S., Sheng, M., & Kim, E. (2001). Sharpin, a novel postsynaptic density protein that directly interacts with the shank family of proteins. *Molecular and Cellular Neurosciences*, 17(2), 385–397. <https://doi.org/10.1006/mcne.2000.0940>
- Lodato, M. A., Rodin, R. E., Bohrsen, C. L., Coulter, M. E., Barton, A. R., Kwon, M., ... Walsh, C. A. (2018). Aging and neurodegeneration are associated with increased mutations in single human neurons. *Science*, 359(6375), 555–559. <https://doi.org/10.1126/science.aao4426>
- Marioni, R. E., Harris, S. E., Zhang, Q., McRae, A. F., Hagenaars, S. P., Hill, W. D., ... Starr, J. M. (2018). GWAS on family history of Alzheimer's disease. *Translational Psychiatry*, 8(1), 1–7.
- Marquand, A. F., Rezek, I., Buitelaar, J., & Beckmann, C. F. (2016). Understanding heterogeneity in clinical cohorts using normative models: Beyond case-control studies. *Biological Psychiatry*, 80(7), 552–561. <https://doi.org/10.1016/j.biopsych.2015.12.023>
- Marschang, P., Brich, J., Weeber, E. J., Sweatt, J. D., Shelton, J. M., Richardson, J. A., ... Herz, J. (2004). Normal development and fertility of knockout mice lacking the tumor suppressor gene LRP1b suggest functional compensation by LRP1. *Molecular and Cellular Biology*, 24(9), 3782–3793. <https://doi.org/10.1128/mcb.24.9.3782-3793.2004>
- Nestor, S. M., Rupsingh, R., Borrie, M., Smith, M., Accomazzi, V., Wells, J. L., ... Bartha, R. (2008). Ventricular enlargement as a possible measure of Alzheimer's disease progression validated using the Alzheimer's disease neuroimaging initiative database. *Brain*, 131(Pt 9), 2443–2454. <https://doi.org/10.1093/brain/awn146>
- Oh, S. J., & Santy, L. C. (2010). Differential effects of Cytohesins 2 and 3 on  $\beta$ 1 integrin recycling. *Journal of Biological Chemistry*, 285(19), 14610–14616. <https://doi.org/10.1074/jbc.M109.043935>
- Orr, A. W., Pedraza, C. E., Pallero, M. A., Elzie, C. A., Goicoechea, S., Strickland, D. K., & Murphy-Ullrich, J. E. (2003). Low density lipoprotein receptor-related protein is a calreticulin coreceptor that signals focal adhesion disassembly. *Journal of Cell Biology*, 161(6), 1179–1189. <https://doi.org/10.1083/jcb.200302069>
- Piers, R. J. (2018). Structural brain volume differences between cognitively intact ApoE4 carriers and non-carriers across the lifespan. *Neural Regeneration Research*, 13(8), 1309–1312. <https://doi.org/10.4103/1673-5374.235408>
- Rantala, J. K., Pouwels, J., Pellinen, T., Veltel, S., Laasola, P., Mattila, E., ... Ivaska, J. (2011). SHARPIN is an endogenous inhibitor of beta1-integrin activation. *Nature Cell Biology*, 13(11), 1315–1324. <https://doi.org/10.1038/ncb2340>
- Sabo, S. L., Ikin, A. F., Buxbaum, J. D., & Greengard, P. (2001). The Alzheimer amyloid precursor protein (APP) and FE65, an APP-binding protein, regulate cell movement. *The Journal of Cell Biology*, 153(7), 1403–1414. <https://doi.org/10.1083/jcb.153.7.1403>
- Saykin, A. J., Shen, L., Yao, X., Kim, S., Nho, K., Risacher, S. L., ... Weiner, M. W. (2015). Genetic studies of quantitative MCI and AD phenotypes in ADNI: Progress, opportunities, and plans. *Alzheimer's & Dementia : The Journal of the Alzheimer's Association*, 11(7), 792–814. <https://doi.org/10.1016/j.jalz.2015.05.009>
- Schuff, N., Woerner, N., Boreta, L., Kornfield, T., Shaw, L. M., Trojanowski, J. Q., ... Weiner, M. W. (2009). MRI of hippocampal volume loss in early Alzheimer's disease in relation to ApoE genotype and biomarkers. *Brain*, 132(Pt 4), 1067–1077. <https://doi.org/10.1093/brain/awp007>
- Sharfe, N., Nikolic, M., Cimpeon, L., Van De Kratts, A., Freywald, A., & Roifman, C. M. (2008). EphA and ephrin-A proteins regulate integrin-mediated T lymphocyte interactions. *Molecular Immunology*, 45(5), 1208–1220. <https://doi.org/10.1016/j.molimm.2007.09.019>
- Skinner, J., Carvalho, J. O., Potter, G. G., Thames, A., Zelinski, E., Crane, P. K., ... Alzheimer's Disease Neuroimaging Initiative. (2012). The Alzheimer's disease assessment scale-cognitive-plus (ADAS-cog-plus): An expansion of the ADAS-cog to improve responsiveness in MCI. *Brain Imaging and Behavior*, 6(4), 489–501. <https://doi.org/10.1007/s11682-012-9166-3>
- Stieglitz, B., Haire, L. F., Dikic, I., & Rittinger, K. (2012). Structural analysis of SHARPIN, a subunit of a large multi-protein E3 ubiquitin ligase, reveals a novel dimerization function for the pleckstrin homology superfold. *Journal of Biological Chemistry*, 287(25), 20823–20829.
- Sudlow, C., Gallacher, J., Allen, N., Beral, V., Burton, P., Danesh, J., ... Landray, M. (2015). UKbiobank: An open access resource for identifying the causes of a wide range of complex diseases of middle and old age. *PLoS Medicine*, 12(3), e1001779.
- Tabatabaei-Jafari, H., Shaw, M. E., Walsh, E., Cherbuin, N., & Alzheimer's Disease Neuroimaging Initiative. (2019). Regional brain atrophy predicts time to conversion to Alzheimer's disease, dependent on baseline volume. *Neurobiology of Aging*, 83, 86–94.
- Tibshirani, R. (1996). Regression shrinkage and selection via the lasso. *Journal of the Royal Statistical Society Series B (Methodological)*, 58(1), 267–288.
- Velayudhan, L., Proitsi, P., Westman, E., Muehlboeck, J. S., Mecocci, P., Vellas, B., ... Simmons, A. (2013). Entorhinal cortex thickness predicts cognitive decline in Alzheimer's disease. *Journal of Alzheimer's Disease*, 33(3), 755–766. <https://doi.org/10.3233/jad-2012-121408>
- Wu, P., Li, M. S., Yu, D. M., & Deng, J. B. (2008). Reelin, a guidance signal for the regeneration of the entorhino-hippocampal path. *Brain Research*, 1208, 1–7. <https://doi.org/10.1016/j.brainres.2008.02.092>
- Xu, L., Groth, K. M., Pearlson, G., Schretlen, D. J., & Calhoun, V. D. (2009). Source-based morphometry: The use of independent component analysis to identify gray matter differences with application to schizophrenia. *Human Brain Mapping*, 30(3), 711–724. <https://doi.org/10.1002/hbm.20540>
- Yushkevich, P. A., Avants, B. B., Das, S. R., Pluta, J., Altinay, M., Craige, C., & Alzheimer's Disease Neuroimaging Initiative. (2010). Bias in estimation of hippocampal atrophy using deformation-based morphometry arises from asymmetric global normalization: An illustration in ADNI 3 T MRI data. *NeuroImage*, 50(2), 434–445.

## SUPPORTING INFORMATION

Additional supporting information may be found online in the Supporting Information section at the end of this article.

**How to cite this article:** Soheili-Nezhad S, Jahanshad N, Gueffi S, et al. Imaging genomics discovery of a new risk variant for Alzheimer's disease in the postsynaptic SHARPIN gene. *Hum Brain Mapp*. 2020;41:3737–3748. <https://doi.org/10.1002/hbm.25083>